Pseudo-spectral Navier-Stokes simulations of compressible Rayleigh-Taylor instability

B. Le Creurer, S. Gauthier
Commisariat à l'Énergie Atomique/Bruyères-le-Châtel, B.P. 12,
91680 Bruyères-le-Châtel Cedex, FRANCE
e-mail : benjamin.le-creurer@cea.fr, serge.gauthier@cea.fr

Abstract

A Fourier-Fourier-Chebyshev pseudo-spectral numerical method for subsonic viscous mixing compressible flows is presented. A multidomain technique with a coordinate transform is used in the vertical direction. The method is self-adaptive: both the location of the numerical interfaces and the coordinate transforms are dynamically adapted through a criterion based on the norm of the calculated solution. The set of collocation points is automatically recalculated in time with the same criterion. A normal mode analysis, with the same numerical method, is also carried out. Dispersion curves and eigenfunctions are obtained for various values of the physical parameters. Results from both the linear and nonlinear regimes of a two-dimensional Rayleigh-Taylor instability are presented.

Key words : Pseudo-spectral methods - Self-adaptive method - Domain decomposition technique - Linear stability analysis - Rayleigh-Taylor Instability.

1 Introduction

Numerical simulations of hydrodynamic instabilities and turbulence require highly accurate numerical schemes. Indeed, in such situations, it is necessary to precisely describe nonlinear interactions between modes of different wave numbers. It is well-known that numerical schemes, especially local methods (*i.e.*, finite differences, finite volumes and finite elements) suffer from various types of errors [15, 16]: the diffusion or dissipative error which is an error on the amplitude of the solution and the dispersion error which is an error on the phase of the solution. Phase error is crucial for hyperbolic equations or the hyperbolic part of a system of equations. This type of error may be quite important with low order schemes. Dissipation error of such schemes is also important and overdamps all the spectrum, especially the high wave numbers. Numerical errors are less important in higher order schemes but

these methods have some difficulties in handling discontinuous solutions such as shock waves or contact discontinuities. Indeed, these schemes require special development for discontinuous solutions. Boundary conditions may be a supplementary difficulty when one uses high order local methods. Indeed, these schemes require a number of ghost nodes which increase with the order of the considered scheme. Spectral methods provide high order discretization procedures with very low dispersion and diffusion errors [12, 2]. Moreover, sophisticated boundary conditions can be easily handled. However, such methods are very sensitive to the Gibbs phenomenon and have some difficulties in handling strong gradients and discontinuities. Recently, some solution techniques have been proposed within the framework of spectral methods for steady and unsteady flows [19, 28, 20, 4, 29].

The project of developing a spectral numerical method for subsonic compressible flows with stiff and unsteady gradients such as those occurring in a Rayleigh-Taylor (RT) instability is carried out step by step. First, a numerical method for compressible thermal convection (*i.e.* an example of compressible flow without strong gradients), has been devised [9, 10]. Numerical simulations of flows with stiff and unsteady gradients require more sophisticated techniques : in these cases, one has to resort to transformation of coordinates. Several difficulties of such methods have been overcome by Guillard and Peyret [14, 13]. These results have been generalized to the multidomain approach [25, 26] and a parallel programming has been performed [6, 7]. The code now solves the complete $3D$ Navier-Stokes equations, with a two-level MPI distribution of the processors.

On the other hand, stability analysis of compressible flows through full numerical simulations is untractable. The large number of flow parameters forbids a careful analysis. Stability analysis within the normal mode analysis is much more convenient since it allows us the investigation of a large number of parameter values. A numerical method for solving the eigenvalue problem which arise from the normal mode analysis has been devised. Such a code provides the dispersion curves (*i. e.* the growth rate of the most unstable mode versus the wavenumber), the eigenfunctions, which give the structure of the flow in the unstable regime, and the so-called Kovásznay modes [3] for various values of the dimensionless parameters of the model [27].

The physical model is given is Sec. 2, the numerical technique is detailed in Sec. 3, the numerical tools are described in Sec. 4 and the simulation results are given in Sec. 5.

2 The physical model

The RT instability generates mixing between fluids. In this paper, mixing of the fluids is described within the single fluid approximation where a third thermodynamic variable, the concentration, denoted c, is introduced. Let us note that such a model does not require a numerical interface or mixed cells. The thermodynamic model uses the "partial pressures - partial densities" formalism in which the pressure p and the density ρ are the sum of the partial pressures and densities of each component, respectively. The local thermal equilibrium hypothesis is assumed, which implies that the temperature is the same for each species. The thermodynamic mixing model writes

$$p = p_1 + p_2, \qquad \rho = \rho_1 + \rho_2, \qquad T = T_1 = T_2, \tag{1}$$

where $\rho_1 = \rho c$, $\rho_2 = \rho(1-c)$ and $p_i = \rho_i \mathcal{R}/\mathcal{M}_i T = (\gamma_i - 1)\,\rho_i\, C_{v_i}\, T$, for $i = 1, 2$. The indices refer to the partial corresponding quantities of fluid constituents 1 and 2. The specific heats at constant volume and constant pressure are C_{v_i} and C_{p_i}. The ratio of specific heats of the mixture, denoted γ, can be evaluated with the help of the following relations

$$\gamma(c) = \frac{C_{p_{mix}}}{C_{v_{mix}}} = \frac{c\,C_{p_1} + (1-c)C_{p_2}}{c\,C_{v_1} + (1-c)C_{v_2}} = \frac{c\,C_{v_1}\gamma_1 + (1-c)C_{v_2}\gamma_2}{c\,C_{v_1} + (1-c)C_{v_2}}. \tag{2}$$

The specific internal energy of the mixture is written

$$e = C_{v_{mix}} T = \left(c\,C_{v_1} + (1-c)\,C_{v_2}\right) T. \tag{3}$$

With these hypothesis, the isentropic sound speed c_S and the Mach number are defined as

$$c_S^2 = \frac{\gamma P}{\rho}, \qquad Ma = \frac{\|\vec{u}\|}{c_S}. \tag{4}$$

The equations for a compressible, viscous, thermally conducting fluid with two miscible components of molecular weights $\mathcal{M}_1$ and $\mathcal{M}_2$ and densities ρ_1 and ρ_2 are as follows

$$\frac{\partial \rho}{\partial t} + \frac{\partial \rho u_j}{\partial x_j} = 0, \tag{5}$$

$$\frac{\partial u_i}{\partial t} + u_j \frac{\partial u_j}{\partial x_j} = -\frac{A_u}{\rho}\frac{\partial p}{\partial x_i} + \frac{B_u}{\rho}\frac{\partial \sigma_{ij}}{\partial x_j} + C_u\,\delta_{i3}, \tag{6}$$

$$\frac{\partial T}{\partial t} + u_j \frac{\partial T}{\partial x_j} = -\frac{A_T}{B_E}\frac{p}{\rho\,C_v}\frac{\partial u_j}{\partial x_j} + \frac{C_T}{B_E}\frac{1}{\rho\,C_v}\sigma_{ij}D_{ij} - \frac{T}{\rho\,C_v}\frac{dC_v}{dc}B_c\frac{\partial^2 c}{\partial x_j x_j} + \frac{B_T}{B_E}\frac{1}{\rho\,C_v}\frac{\partial^2 T}{\partial x_j x_j}, \tag{7}$$

$$\frac{\partial c}{\partial t} + u_j \frac{\partial c}{\partial x_j} = \frac{B_c}{\rho}\frac{\partial^2 c}{\partial x_j x_j}. \tag{8}$$

The system of equations is closed with the equation of state

$$p = \rho\,T\,\left(1 + r - 2\,r\,c\right), \tag{9}$$

where $r = (\mathcal{M}_1 - \mathcal{M}_2)/(\mathcal{M}_1 + \mathcal{M}_2)$. The three components of the velocity are u_i for $i = 1, 2, 3$, and $x_1 = x$, $x_2 = y$, $x_3 = z$. The reference value for the specific heat C_v is $C_{v,r}$. The components σ_{ij} of the viscous stress tensor $\bar{\bar{\sigma}}$ are defined in the Stokes approximation by $\sigma_{ij} = \partial_i u_j + \partial_j u_i - 2/3\,\delta_{ij}\partial_\ell u_\ell$, where and $i, j, \ell = 1, 2, 3$. The coefficients appearing in Eqs.(5)-(8) will be specified later. Velocity, temperature and concentration boundary conditions could be either of Dirichlet, Neumann or Robin type. No boundary conditions are applied on the density or the pressure fields.

2.1 The Rayleigh-Taylor flow

The basic state is found by assuming the hydrostatic equilibrium in the upper and lower fluids, with a constant temperature. The density profile is smoothed by using the functions $\mathrm{H}_{\pm}(z) =$

$1/2\,(1 \pm \mathrm{erf}\,(z/\delta))$, where the parameter δ represents the width of the central gradient of the density. It comes

$$\begin{aligned}
\overline{\rho}(z) &= (1-r)\exp(A_+\,z)\,\mathrm{H}_+(z) + (1+r)\exp(A_-\,z)\,\mathrm{H}_-(z)\,,\\
\overline{c}(z) &= (1+r)\exp(A_-\,z)\,\mathrm{H}_-(z)\,/\overline{\rho}(z),\\
\overline{p}(z) &= \overline{p}_b + (1-r^2)\left[\exp(A_+\,z)\,\mathrm{H}_+(z) + \exp(A_-\,z)\,\mathrm{H}_-(z)\right.\\
&\quad - \exp\left(A_+^2\delta^2/4\right)\frac{1}{2}\mathrm{erf}\left(z - A_+\delta^2/2\right)\\
&\quad \left.+\exp\left(A_-^2\delta^2/4\right)\frac{1}{2}\mathrm{erf}\left(z - A_-\delta^2/2\right)\right] \qquad (10)\\
\overline{T}(z) &= \overline{p}(z)/\left[\overline{\rho}(z)\,(1+r-2r\overline{c}(z))\right],
\end{aligned}$$

where $A_\pm = C_u/\left(2\,A_u\,(1 \pm r)\right)$. The constant $\overline{p}_b$ is adjusted in such a way that $\overline{p}(z_{bottom}) = 1$. We used for the reference length L_x, the horizontal width of the computational box, $t_r = (L_x/g)^{1/2}$ for the time reference with $\vec{g} = (0, 0, -g)$. The reference of velocity is then $U_r = (L_x g)^{1/2}$. According to these reference scales, the dimensionless coefficients for the Navier-Stokes equations (5)-(9) are given in Table I, where Re is the Reynolds number, Sc the Schmidt number, Pr the Prandtl number and $Sr = RT_r/(g\,L_r)$ stands for the stratification parameter of the steady state configuration.

A_{u_i}	B_{u_i}	$C_{u_{1,2}}$	C_{u_3}	A_T	B_T	C_T	A_E	B_E	C_E	B_c
Sr	$\dfrac{1}{Re}$	0	-1	$(\gamma-1)$	$\dfrac{\gamma}{RePr}$	$\dfrac{\gamma-1}{ReSc}$	$\dfrac{\gamma-1}{Sr}$	1	$-A_E$	$\dfrac{1}{ReSc}$

Table I: Dimensionless coefficients of the Navier-Stokes equations for the Rayleigh-Taylor flow.

3 The numerical technique

In a spectral method, all physical quantities are expanded on a basis of orthogonal functions. These functions are non-zero all over the computational domain as opposed to functions of expansion used in finite volume, finite difference or finite element methods which are localized in space. Fourier functions may be chosen but they are restricted to periodic functions. Polynomial expansions have to be preferred in inhomogeneous configurations and, in practice, Chebyshev and Legendre polynomials are used. In a collocation method spatial derivatives are computed in the spectral space and nonlinear products are performed in the physical space (pseudo-spectral method). Numerical analysis of these methods are given in Refs [22, 2, 12]. For RT type flows, and many other flows, assuming one or two periodic directions is a reasonable approximation. As a result, we choose a Fourier-Fourier-Chebyshev basis as the functions of expansion. All physical variables are then expanded as

$$\psi(x,y,z,t) = \sum_{\ell=-L}^{L}\sum_{p=-P}^{P}\sum_{q=0}^{Q-1}\psi_{\ell\,p\,q}(t)\,T_q\left(\xi\,(z)\right)\,e^{2\mathbf{i}\pi\left(\frac{\ell}{L}x+\frac{p}{P}y\right)} \qquad \text{where} \qquad -1 \le \xi \le 1. \qquad (11)$$

In (11) $T_q(\xi)$ denotes the q-th Chebyshev polynomial for the ξ variable. The most general set of Chebyshev collocation points is given by a set of M subdomains in which a coordinate transform is used. Each coordinate transform depends on one parameter denoted for the m-th subdomain $a^{(m)}$ and it reads

$$z^{(m)}(\xi) = z_{ave}^{(m)} + a^{(m)}\,\xi\left(1 + {b^{(m)}}^2 - \xi^2\right)^{-1/2} \quad \text{where} \quad m = 1,\ldots,M, \qquad z_{inf}^{(m)} \le z^{(m)} \le z_{sup}^{(m)}. \tag{12}$$

The parameters $a^{(m)}$ are real and positive. The constants $z_{ave}^{(m)}$ and $b^{(m)}$ are defined by $z_{ave}^{(m)} = \frac{1}{2}\left(z_{inf}^{(m)} + z_{sup}^{(m)}\right)$ and $b^{(m)} = 2a^{(m)}/\left(z_{sup}^{(m)} - z_{inf}^{(m)}\right)$, respectively. Let us list the parameters which define this set of collocation points. The number of collocation points is given by the M integers Q_i, where $i = 1,\ldots,M$. The location of the boundaries of the subdomains are defined by $M+1$ real parameters and there are M coordinate transform parameters. As a result, the set of collocation points is defined by $3M+1$ parameters. Since some of them are kept fixed for a given simulation, only $2M-1$ real parameters have to be determined when the set of collocation points is redefined. It has been shown that these parameters can be determined automatically by minimizing some norm of the calculated solution [1, 14, 13, 25, 26]. This numerical procedure has been developed over the last fifteen years. First, Guillard and Peyret [14] introduced an adaptive procedure in which a coordinate transform was chosen to minimize the weighted Sobolev norm H^2_ω of the solution. These adaptive methods are based on the following inequality

Theorem 1 *For any σ and μ such that $1 \le \mu \le \sigma$, there exists a constant C such that*

$$\|u - P_N(u)\|_{\mu,\omega} \le C(\sigma)\, N^{2\mu-\sigma-\frac{1}{2}}\, \|u\|_{\sigma,\omega}\,, \tag{13}$$

where

$$\|u\|^2_{\sigma,\omega} = \sum_{i=0}^{\sigma} \int_{-1}^{+1} \left|\frac{d^i u}{d\xi^i}\right|^2 \omega(\xi) d\xi \quad \text{with} \quad \omega(\xi) = 1/\sqrt{1-\xi^2}.$$

This theorem means that the projection error in the H^σ_ω Sobolev space is bounded by the norm of the function $\|u\|_{\sigma,\omega}$. It turns out that the value $\sigma = 2$ gives good results. This numerical method was proven to be efficient to compute one-dimensional premixed flame and two-dimensional plane flame moving into a reactive medium. This numerical procedure was successfully used to simulate temporally growing compressible mixing layers. In Refs. [25, 26] these results were generalized to the multidomain approach and we shown that the criterion based on the minimum of the H^2_ω-norm may also be used to determine the best location of the subdomain interfaces. An example is given in Fig.1 where the influence of the location of the interface appears clearly. In this figure, we have plotted the norm of the approximation J_2 for the function $\sin x_3/x_3$ versus the location of the interface $x_{3,interface}$ in a 3-subdomain calculation. The norms of the function in the outer and inner subdomains are given by the dashed line. The total norm represented with a solid line exhibits clearly a minimum at $x_{3,interface} \simeq 5.70$. This is the location of the subdomain boundary which leads to the bestsmallest interpolation error of the test function.

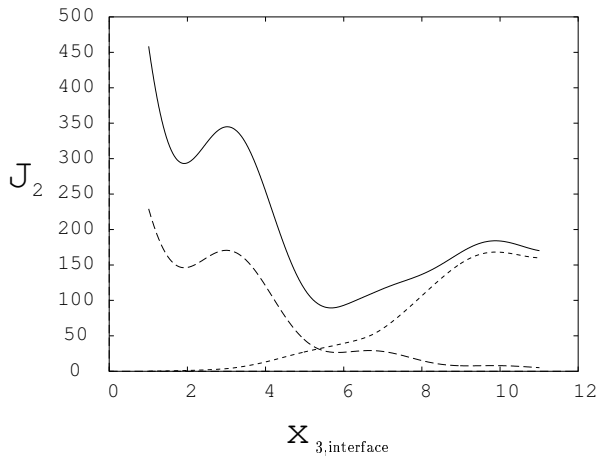

Figure 1: The norm of the approximation J_2 for the function $\sin x_3/x_3$ versus the location of the interface $x_{3,interface}$ in a 3-subdomain calculation. The number of collocation points is 51 in each subdomain. The interfaces are initially located at ± 6. The norms of the function in the outer and inner subdomains are given by the dashed lines. The solid line stands for the total norm. The total norm exhibits a minimum at $x_{3,interface} \simeq 5.70$.

A simple and robust procedure have been used to determine the best location of the interfaces. This algorithm consists in calculating the norm of the test function for some selected values ofthe numerical interface between subdomains. The best location of this interface is given by the minimum of the norm of the test function. Such computation is done for every interface and iterated up to convergence, *i.e.*, when fixed values for the interface locations have been reached. The number of iterations depends upon the number of subdomains. However, it turns out that 4 or 5 iterations are usually enough to achieve convergence. After convergence, a new set of Chebyshev collocation points has been defined. The solution is then interpolated on this new set of collocation points. In a numerical simulation this adaption is carried out dynamically in order to follow the strong gradients. More precisely, we used the following criterion: whenever the norm of the test function increases by some factor (typically 3% in one of the M subdomains) the dynamical procedure is carried out. Comparisons have been made, on the temporal Kelvin-Helmholtz flow, against more classical methods, *i.e.*, finite volume methods and prove the superiority of such spectral techniques [11].

4 The numerical tools

4.1 The linear stability code

The linear stability analysis is carried out within the normal mode analysis [8, 27]. In this approach, variables are supposed to behave as

$$\phi(x,z,t) = \overline{\phi}(z) + \widehat{\phi}(z)\, e^{\mathbf{i}k\,x}\, e^{\sigma\,t}, \tag{14}$$

where $\phi^t = (\rho\, u_i\, T\, c)$. The quantities $\overline{\phi}$ and $\widehat{\phi}$ are the basic state and the perturbation, respectively. The wavenumber is k and the complex growth rate of the perturbation is σ. The initial value problem

of the linearized complete Navier-Stokes equations leads to an eigenvalue problem which writes

$$A\,\widehat{\phi} = \sigma\, B\,\widehat{\phi}, \tag{15}$$

where the matrices A and B are 5×5 block matrices for a 2D calculation. These matrices depend on the basic state (10) and on the first and second derivative operators, D and D^2 respectively. The matrix B contains the boundary and the matching conditions.

The features of our numerical code are the following ones :

- Pseudo-spectral, multidomain method with self-adaptive generation of the collocation points. The test function is choosen to be equal to

$$\mathcal{F}[\rho, c, T] = \frac{\overline{\rho}}{\overline{\rho}_{\max}} + \frac{\overline{T}}{\overline{T}_{\max}} + \frac{\overline{c}}{\overline{c}_{\max}} \tag{16}$$

  where $\overline{\rho}$, $\overline{T}$ and $\overline{c}$ are given by Eqs.(10).

- The boundary conditions are the same as in a full simulation, *i. e.*, two homogeneous Dirichlet boundary conditions are imposed on the vertical velocity v while homogeneous Neumann boundary conditions are applied on the horizontal velocity u, the temperature T and the concentration c. There is no boundary conditions on the density ρ.

- We require the continuity of the function and its first derivative for the velocity, temperature and concentration. Matching are performed with the penalty method which reads

$$\Gamma_1 \left[\widehat{\phi}^t_m(\xi_N) - \widehat{\phi}^t_{m+1}(\xi_1) \right] = 0, \tag{17}$$

$$\Gamma_2 \left[\frac{d\widehat{\phi}^t_m}{dz}(\xi_N) - \frac{d\widehat{\phi}^t_{m+1}}{dz}(\xi_1) \right] = 0, \tag{18}$$

  for $m = 1, \cdots, M-1$ and $\Gamma_{1,2}$ are two arbitrary constants. For the density, only the continuity of the function is required through Eq.(17).

- It provides eigenvalues (growth rate), eigenfunctions, dispersion curves and Kovásznay modes (acoustic, entropy and vorticity).

4.1.1 Local eigenvalue search

The eigenvalue problem (15) is usually solved with a global LZ method [17, 18] available through the IMSL librairy which provides both the eigenvalues and the eigenvectors. However in some cases, the accuracy of such procedure is not good enough and one has to resort to the inverse Rayleigh iterations which is a more powerful and accurate method. For the generalized eigenvalue problem, this algorithm reads ([30], p.635):

$$(A - \sigma_q\, B)\ \widehat{\phi}^{(q+1)} = B\,\widehat{\phi}^{(q)} \tag{19}$$

$$\left(A^T - \sigma_q\, B^T\right)\ \widehat{\psi}^{(q+1)} = B^T\,\widehat{\psi}^{(q)}. \tag{20}$$

At the end of the iterations the eigenfunction and its adjoint are normalized:

$$\widehat{\phi}^{(q+1)} = \widehat{\phi}^{(q+1)} / \max\left(\widehat{\phi}^{(q+1)}\right), \tag{21}$$

$$\widehat{\psi}^{(q+1)} = \widehat{\psi}^{(q+1)} / \max\left(\widehat{\psi}^{(q+1)}\right), \tag{22}$$

and the eigenvalue is obtained from:

$$\sigma_{q+1} = \frac{\left(\widehat{\psi}^{(q+1)}, A\,\widehat{\phi}^{(q+1)}\right)}{\left(\widehat{\psi}^{(q+1)}, B\,\widehat{\phi}^{(q+1)}\right)}. \tag{23}$$

The full complex linear systems (19)-(21) are solved with a LU factorization. The Numerical Recipes routines has been rewritten as complex routines as recommended in Ref.[23]. The initial guess for the iterations is obtained either from a LZ calculation or from an analytical model [5, 21].

4.1.2 Validation of the linear analysis

The whole method has been validated on various perfect fluid configurations where the exact solution is known [21]. We present here one case where the Atwood number is $A_t = 0.99$ (*i.e.* density ratio is equal to 199). The density profile of this configuration is displayed in Fig.2 (left). The eigenvalue

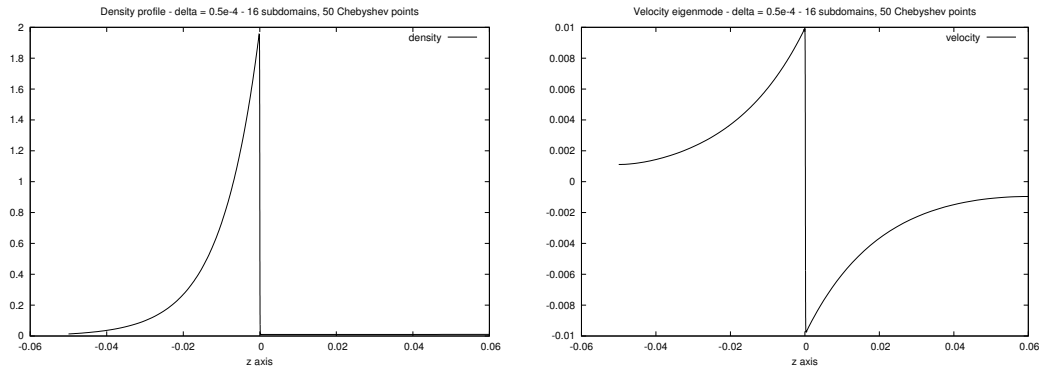

Figure 2: Perfect fluid Atwood=0.99 - density profile (left) and horizontal velocity eigenmode (right).

obviously depends on the numerical width of the gradient δ (Eqs.(10)) and we have carried out several calculations versus this parameter. Extrapolation of the eigenvalue at $\delta = 0$ gives the value $\sigma(\delta = 0)$, which compared with the exact solution leads to an accuracy of 10^{-4}. Calculations have been carried out with 16 suddomains with 50-Chebyshev polynonials in each. The eigenmode of the horizontal velocity has been plotted in Fig. 2 (right). Let us emphasize that these two profiles are continuous, although very stiffs, that shows the capability of the numerical method to handled strong gradients. Figure 3 displays the density profile for a viscous configuration with an Atwood number equal to 0.10. The spatial resolution, for this configuration, is 5×64 Chebyshev polynomials. Figure 4 is an example of a dispersion curve obtained for the following values of the Atwood, Reynolds and stratification numbers : $A_t = 0.2$, $Re = 400$ and $Sr = 25$. The Schmidt, Prandtl and adiabatic index are 20, 2 and

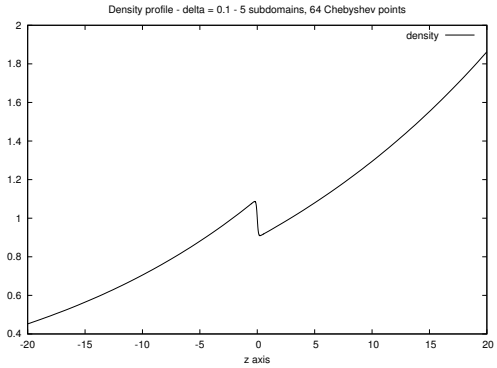

Figure 3: Viscous fluid Atwood=0.10 - density profile.

5/3, respectively. It shows that the physical model (5)-(9) previously described, exhibits a cut-off wave number (mainly due to species diffusion) beyond which the RT-flow is stable. As a result, there exists a wavenumber for which the — real — growth rate is maximum. These results have been obtained with 5×64 Chebyshev polynomials.

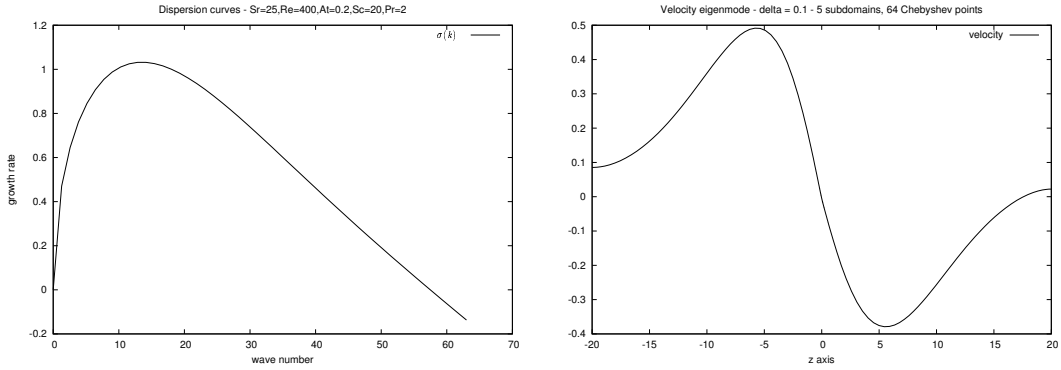

Figure 4: Viscous fluid Atwood=0.10 - Dispersion curve (left) and horizontal velocity eigenmode (right).

4.2 The code for the complete Navier-Stokes equations

The features of the numerical method are the following ones :

- **A**daptive **M**ultidomain ps**E**udospectral **N**umerical meth**O**d for **P**arallelization of **H**ydrodynamic **I**nstabilities **S**imulation.
- 3D complete Navier-Stokes equations, single fluid approximation,
- Discretisation in space: expansion in Fourier series (x, y) and Chebyshev polynomials (z), Discretisation in time: Semi-implicit 3-step 2nd order Runge-Kutta scheme,
- Multidomain in the vertical direction,
- Location of the frontiers are self-adaptive,

- Self-adaptive coordinate transform in each subdomain,
- Density matching : Upwind method
  Velocity, temperature and concentration matching : Influence matrix technique [24],
- MPI-Parallel programmation with multicommunicator.

5 Simulation results

A 2D simulation for the same set of parameter values used in the linear theory has been carried out, *i.e.*, $A_t = 0.2$, $Re = 400$, $Sr = 25$, $Sc = 20$, $Pr = 2$ and $\gamma = 5/3$. The spatial resolution is $n_x = 128$ and $n_z = 5 \times 64$. This caculation has been performed on a HP/COMPAQ parallel calculator with EV68 alpha scalar processors. This caculation used 40 processors.

A perturbation is introduced in the density profile, which writes for the single mode case

$$\rho\,(x,z) = \rho\left(x, z - \varepsilon\,\mathrm{e}^{-k\,|z|}\cos k\,x\right), \tag{24}$$

where ε and k are the amplitude and the wavenumber of the initial perturbation, with the numerical values $\varepsilon = 0.10$ and $k = 2\,\pi$. The same expression is used for the initial concentration profile.

Figures 5 and 6 represent the evolution of the mesh vs. time. we see clearly the numerical interfaces which follow the main gradients of the flow. The isocontours of the concentration coloured with the vorticity are also shown. Figures 7 and 8 give the isocontours of the concentration coloured with the vorticity without the mesh. It is a classical single mode RT-pattern. The calculation is pursued until the mushroom reaches the bottom of the box. Then gradients of concentration begin to settle down. Figures 9 and 10 display the isocontours of the vorticity. Figure 11 displays the 3D plots of the mean value — averaged in the x-direction — of the concentration, $c(z,t)$ (left) and the r.m.s. value of the vertical velocity $w_{rms} = \sqrt{\overline{w^2}}$ (right). We see clearly the concentration gradients flattening versus time although the calculation has been stopped before the end of the physical process. Note that the symetry with respect to the middle of the box is been lost at the end of the calculation ($t = 36$).

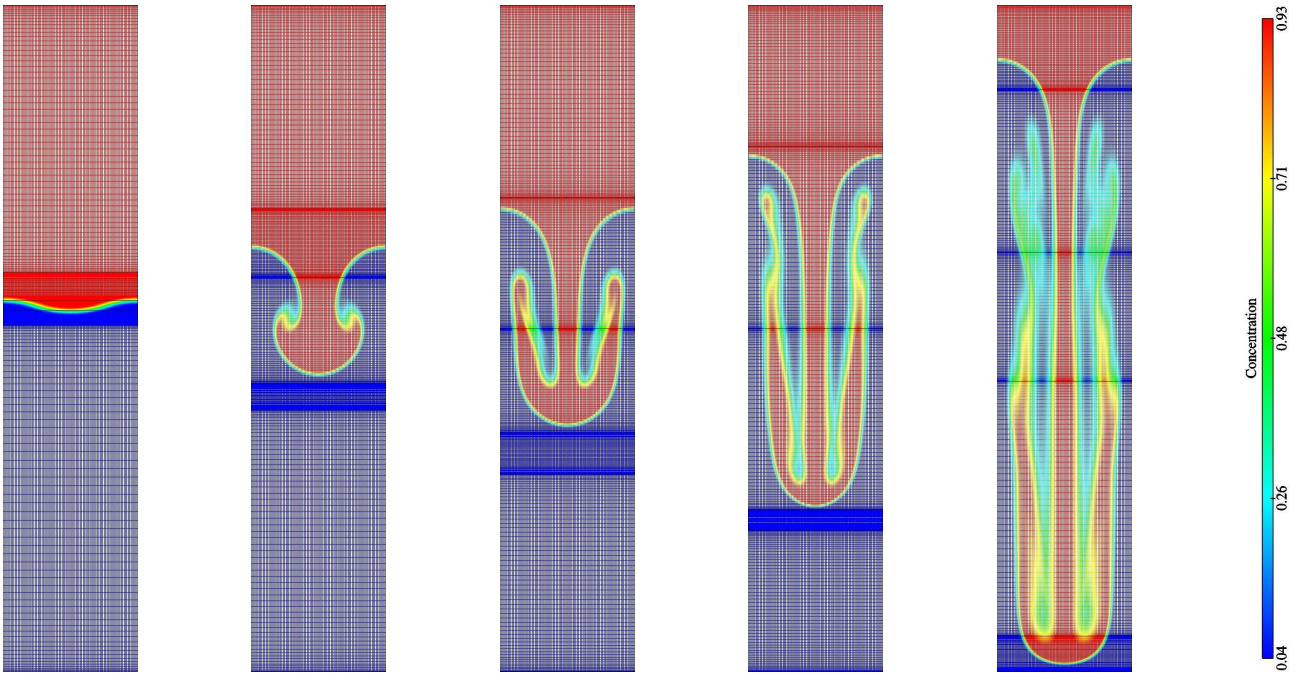

Figure 5: Evolution of the mesh and the numerical interfaces in the z-direction, at selected times $t = 0$, 4.5, 6.8, 9.8 and 15. The isocontours of the concentration are coloured with the density.

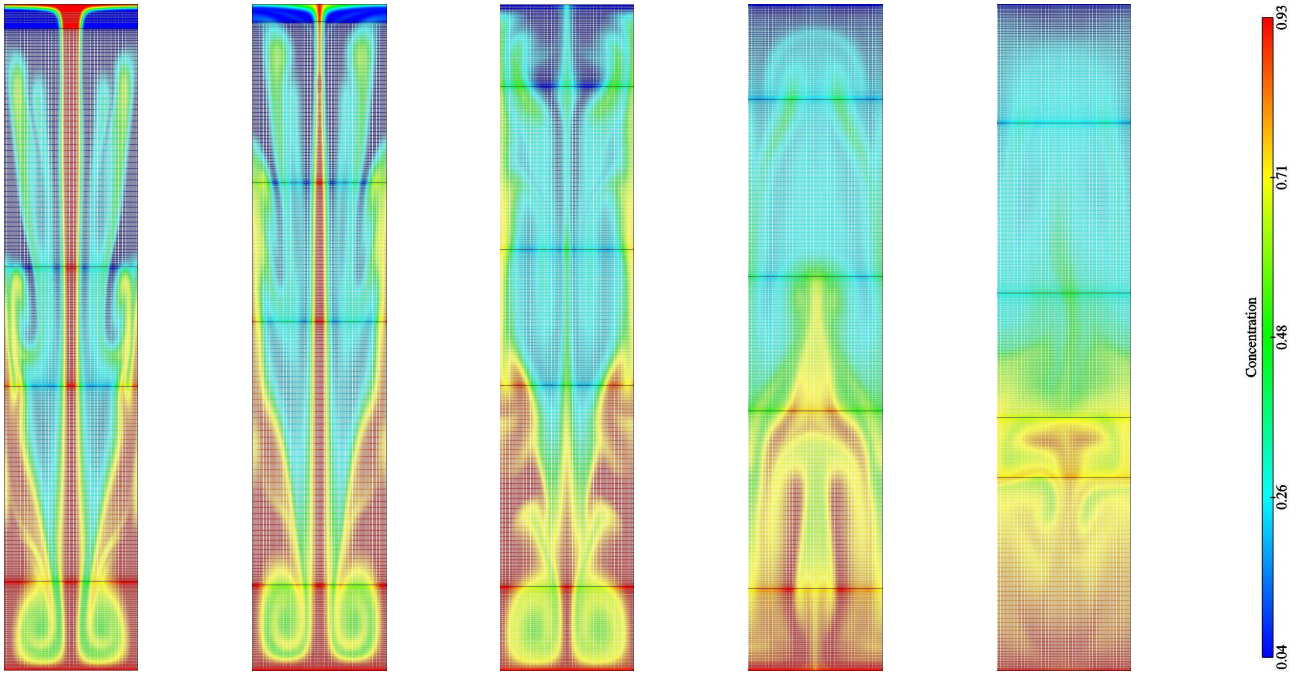

Figure 6: Same as in Fig.5 at times $t = 19$, 22, 25.5,36.7 and 47.

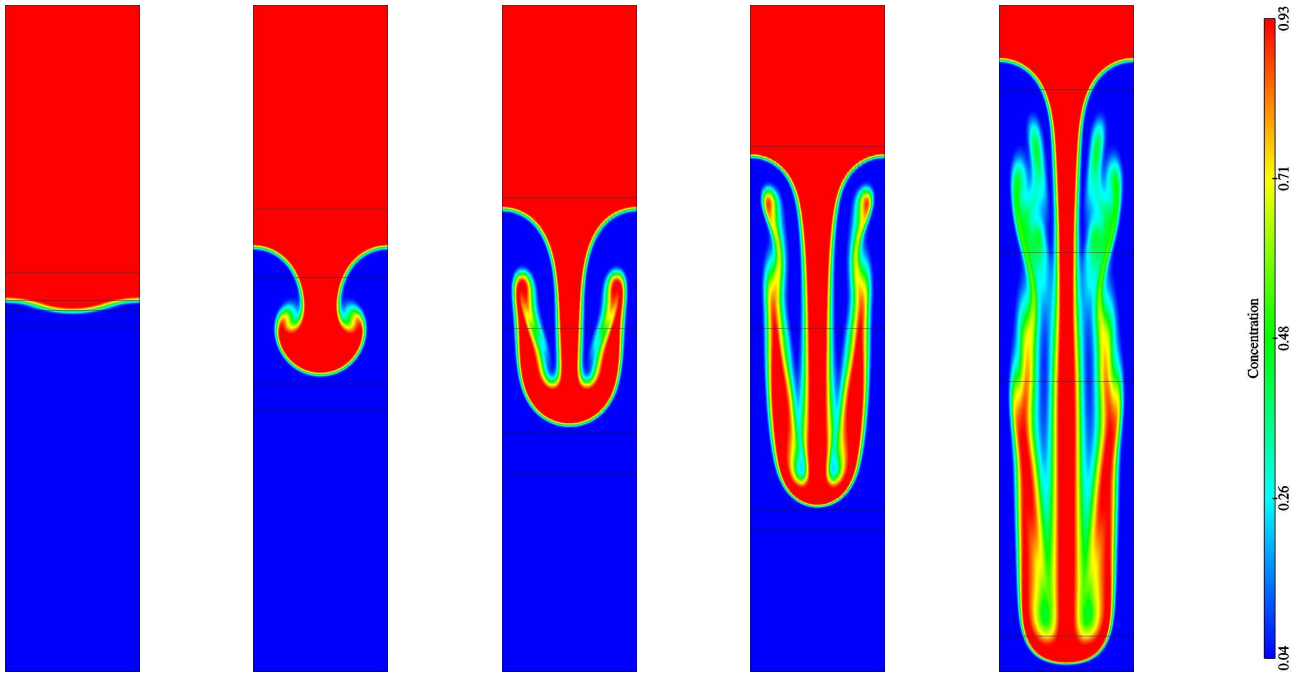

Figure 7: Same as in Fig.5 without the mesh.

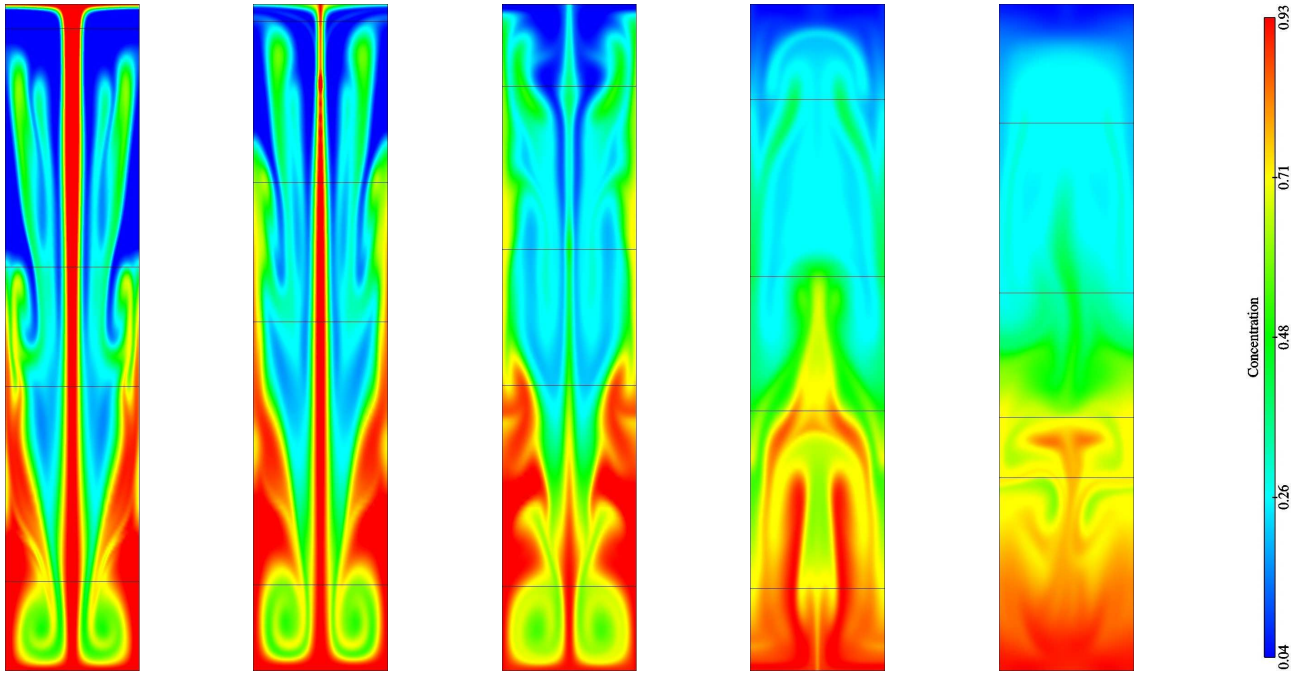

Figure 8: Same as in Fig.6 without the mesh.

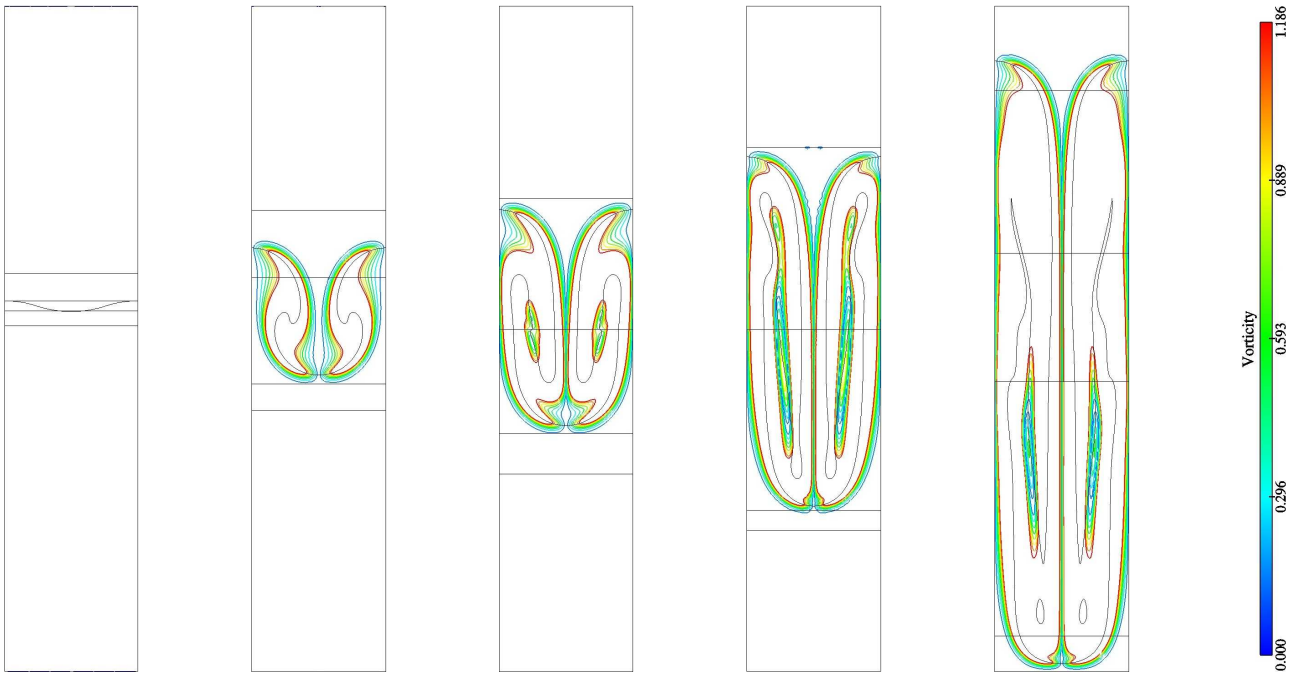

Figure 9: Isocontours of the vorticity at selected times $t = 0$, 4.5, 6.8, 9.8 and 15.

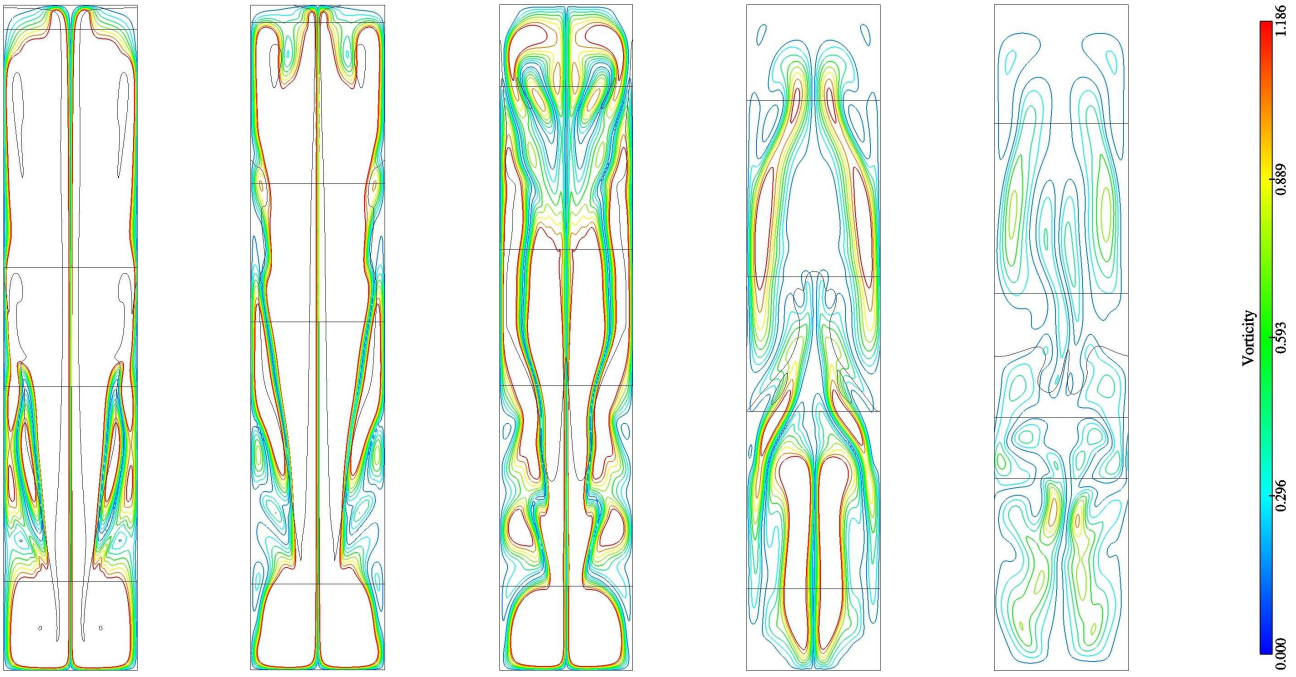

Figure 10: Same as in Fig.9 at selected times $t = 19$, 22, 25.5, 36.7 and 47.

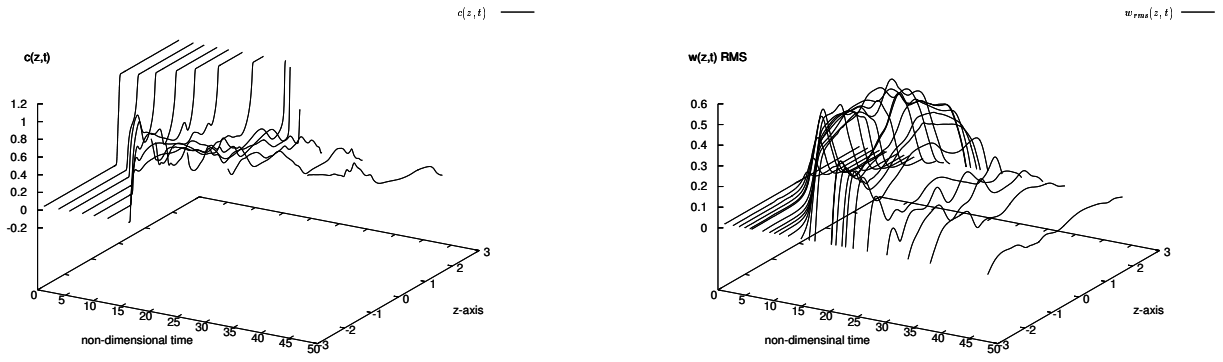

Figure 11: Spatio-temporal diagram of the mean value — averaged in the x-direction — of the concentration, $c(z,t)$ (left) and the r.m.s. value of the vertical velocity $w_{rms} = \sqrt{\overline{w^2}}$ (right).

6 Concluding remarks

We have presented a Fourier-Fourier-Chebyshev pseudo-spectral numerical method for subsonic viscous mixing compressible flows. This method is based on a dynamical multidomain decomposition, *i.e.*, the location of the numerical interfaces and the coordinate transforms are dynamically adapted through a criterion based on the norm of the calculated solution. A stability analysis code, based on the same method, has also been devised. Dispersion curves and eigenfunctions are obtained for various values of the physical parameters. Results from both the linear and nonlinear regimes of a two-dimensional Rayleigh-Taylor instability have been presented. The next step is now to carry out 3D calculations with single- and multimode initial perturbations.

References

[1] A. Bayliss and B.J. Matkowsky. Fronts relaxation oscillations, and period doubling in solid fuel combustion. *J. Comput. Phys.*, 71:147–168, 1987.

[2] C. Canuto, M.Y. Hussaini, A. Quarteroni, and T.A. Zang. *Spectral Methods in Fluids Dynamics.* Springer-Verlag, 1988.

[3] B.-T. Chu and L. S. G. Kovásznay. Non-linear interactions in a viscous heat-conducting compressible gas. *J. Fluid Mech.*, 3:494–514, 1957.

[4] W.S. Don. Numerical simulation of shock-cylinder interactions. *J. Comput. Phys.*, 110:103, 1994.

[5] R.E. Duff, F.H. Harlow, and C.W. Hirt. Effects of diffusion on interface instability between gases. *Phys. Fluids*, 5:417, 1962.

[6] É. Fournier. *Méthodes spectrales, méthodes de décomposition de domaines et parallélisme : Application aux instabilités de Rayleigh-Taylor.* PhD thesis, CEA-Université de Paris VI, 1998.

[7] É. Fournier, S. Gauthier, and F. Renaud. 2d pseudo-spectral parallel navier-stokes simulations of compressible rayleigh-taylor instability. *Comput. & Fluids*, 31:569, 2001.

[8] A. Gauthier, S. Gamess and G. Iooss. Chaotic behavior in oscillatory compressible convection in extended boxes for small prandtl numbers. *Europhys. Lett.*, 13:117–122, 1990.

[9] S. Gauthier. A spectral collocation method for two-dimensional compressible convection. *J. Comput. Phys.*, 75:217, 1988.

[10] S. Gauthier. A semi-implicit collocation method : Application to thermal convection in 2d compressible fluids. *Int. J. Num. Meth. in Fluids*, 12:985, 1991.

[11] S. Gauthier, H. Guillard, T. Lumpp, J.-M. Malé, R. Peyret, and F. Renaud. A spectral domain decomposition technique with moving interfaces for viscous compressible flows. In J.-A. Désidéri, C. Hirsch, P. Le Tallec, M. Pandolfi, and J. Périaux editors, editors, *Proceedings of the Third ECCOMAS Computational Fluid Dynamics Conference*, pages 839–844, 1996.

[12] D. Gottlieb and S.A. Orszag. Numerical analysis of spectral methods: Theory and applications. *SIAM, Philadelphia*, 1977.

[13] H. Guillard, J.M. Male, and R. Peyret. Adaptative spectral methods with application to mixing layer computation. *J. Comput. Phys.*, 102:114–127, 1992.

[14] H. Guillard and R. Peyret. On the use of spectral methods for the numerical solution of stiff problems. *Comput. Methods Appl. Mech. Eng.*, 66:17–43, 1988.

[15] C. Hirsh. *Numerical Computation of Internal and External Flows.* John Wiley & Sons, New York, 1988.

[16] L. Jameson. High order schemes for resolving waves: Number of points per wavelength. *J. Comput. Phys.*, 15:417–439, 2000.

[17] L.C. Kaufman. The lz algorithm to solve the generalized eigenvalue problem. *SIAM J. Num. Anal.*, 11:997–1023, 1974.

[18] L.C. Kaufman. The lz algorithm to solve the generalized eigenvalue problem. *ACM Trans. Math. Software*, 1:271–281, 1975.

[19] D. Kopriva. A spectral multidomain method for the solution of hyperbolic systems. *Applied Num. Math.*, 2:221, 1986.

[20] D. Kopriva. Multidomain spectral solution of compressible viscous flows. *J. Comput. Phys.*, 115:184, 1994.

[21] W.G. Matthews and G.R. Blumenthal. Rayleigh-Taylor stability of compressible and incompressible radiation-supported surfaces and slabs : application to qso clouds. *Ap. J.*, 214:10–20, 1977.

[22] R. Peyret. *Spectral Methods For viscous incompressible flows*. Springer-Verlag, 2002.

[23] W. H. Press, S. A. Teukolsky, W. T. Vetterling, and B. P. Flannery. *Numerical recipes*. Cambridge University Press, Cambridge, UK, 2 edition, 1994.

[24] J.-P. Pulicani. A spectral multidomain method for the solution of 1-D-Helmholtz and stokes-type equations. *Computers and Fluids*, 16:207, 1988.

[25] F. Renaud. *Méthode spectrale de décomposition dynamique de domaines : Application aux écoulements compressibles de Rayleigh-Bénard et Kelvin-Helmholtz*. PhD thesis, CEA-Université de Nice-Sofia antipolis, 1996.

[26] F. Renaud and S. Gauthier. A dynamical psudo-spectral domain decomposition technique: application to viscous compressible flows. *J. Comput. Phys.*, 131:89–108, 1997.

[27] É. Serre and S. Gauthier. An auto-adaptative multi-domain pseudo-spectral technique for linear stability analysis : application to viscous compressible flows. *J. Sci. Comput.*, 17:153–165, 2002.

[28] D. Sidilkover and G.E. Karniadakis. Non-oscillatory spectral element chebyshev method for shock wave calculations. *J. Comput. Phys.*, 107:10, 1993.

[29] A. Suresh. An assessment of spectral nonoscillatory schemes. *J. Comput. Phys.*, 114:339, 1994.

[30] J. H. Wilkinson. *The algebraic eigenvalue problem*. Oxford University Press, Oxford, UK, 1965.

Contents